Modelling Signal Generation in CVD Diamond Detectors

David Fish

April 19, 1997

Abstract

Chemical vapor deposition (CVD) diamond detectors offer a potential alternative to silicon for particle tracking close to the interaction region of high energy collider experiments. The most outstanding advantage of diamond over silicon is its radiation hardness. Whereas silicon is predicted to degrade to an unusable state within a year or two of operation at future luminosities, current studies show that diamond may last an order of magnitude longer. However, diamond detectors currently have the problem of low signal to noise ratio primarily due to a relatively small charge collection distance. The development of a computer model of these detectors has aided in the understanding of currently available diamond and will hopefully make predictions as to how new diamond could be used to make superior detectors in the future.

1 Introduction – diamond vs. silicon

At collider facilities, detectors are needed near the interaction region in order to track the trajectories of charged particles. Whereas silicon detectors provide a known and proven technology for charged particle detection, diamond detector technology is still in the development stage both in manufacturing and in the understanding of the basic physics of charge transport processes. The superior radiation hardness and other properties of diamond make it a potentially attractive alternative to silicon. This thesis discusses the investigations made of charge transport phenomena in diamond. Once a working model is in hand, predictions can be made for other detectors. Thus, the model may eventually be used to determine optimal operational parameters as well as to advance knowledge of charge transport for CVD diamond detectors.

1.1 Microstrip detectors

Near the interaction region at detectors at hadron colliders, vertex detectors are needed to determine the trajectory of particles coming from the interaction region, so that the exact point of origin, or vertex, of a jet may be found. Perhaps one of the most important applications of this is in looking for the displaced vertices characteristic of b jets. In order to determine this trajectory, microstrip detectors are used. The detectors have either one or both sides covered with microstrips – strips of metal approximately 25 μm wide, separated by a distance of typically 50-100 microns. A potential is applied between the two sides of the detector. The electrons and holes liberated by ionization from the passage of a particle through the bulk of the material are swept to opposite sides by the applied potential. The movement of the charges induces a signal on the strips. The distribution of signals seen on the strips determines the location of the incident particle's passage through the detector. Using several such detectors, the trajectory may be found.

The basic operation of microstrip detectors is different as well. For silicon, a p-n junction is formed by appropriate doping. Operating at reverse bias, electron-hole pairs liberated by the passage of a charged particle through the charge depletion region, drift towards the junction. The active region is made as wide as possible through high p-doping in a narrow region and small n-doping in a wide region[1]. Diamond on the other hand, acts as a resistor. The liberated charges drift only because of the external electric field applied between the two sides of the detector.

1.2 What is CVD diamond?

Chemical vapor deposition (CVD) diamond is a type of artificial diamond which is created by the deposition of carbon onto a substrate specifically designed to induce carbon crystal growth in the form of diamond, rather than in the more enegetically favorable form, graphite. Whereas natural diamond grows as one large crystal, CVD diamond grows as a collection of microcrystals.

1.3 Collection distance and mean path length

One of the quantities used in discussing solid state detectors, the collection distance, d_c, is defined as the average distance an electron-hole pair, liberated by the passage of a charged particle through the detector, will separate under the influence of an applied electric field. The maximum value the collection distance can take is the thickness of the detector. This is in fact the value of the collection distance in a silicon detector. Because the ratio of induced charge to deposited charge is exactly equal to d_c/t, where t is the thickness of the detector, silicon detectors collect all of the deposited charge, thus giving maximum signal to noise ratios and, consequently, excellent spatial resolution.

A quantity which is perhaps more physically meaningful than the collection distance is the mean path length, denoted λ_e or λ_h for electrons and holes, respectively. This is defined to be the average distance that an electron or hole will travel before coming to rest in the detector. Unlike the collection distance, this number is *independent* of the thickness of the detector, and is purely a property of the bulk of the material. Since the mean path length is proportional to the charge carrier lifetime, the mean is over an exponential distribution. For the purposes of the model, it is assumed that the mean path lengths of electrons and holes are equal. This common mean path length will be denoted λ_q.[1]

For a small λ_q detector such as diamond, the amount of charge collected at the strips increases with λ_q. However, because the mean path length refers to the mean of an exponential distribution, even when the mean path length equals the physical thickness of the detector, the collected charge will *not* equal the deposited charge. Only in the case of an infinite mean path length will all the deposited charge be collected.

The most significant obstacle to making diamond into a viable detector for experiments are the characteristically *finite* electron and hole mean path lengths. The small mean path lengths also correspond to small collection distances. However, as CVD diamond grows thicker, the single crystal size in the diamond also grows larger. [2] The collection distance apparently varies proportionally with crystal size. Current studies are being made with very thick detectors with large average collection distance.

Although a thick detector will generally have greater signal due to greater charge deposition, such a detector is not well suited for use in an experiment both because of space considerations and its tendency to interfere with the trajectory of an incident particle. "Lapping" off material from the low mean path length side of a thick detector will hopefully leave behind a thin detector with a mean path length and a collection distance comparable to the remaining thickness.

1.4 Desirable properties of diamond

Although silicon microstrip detectors are expected to degrade to an unusable state within a few years of operation at the current fluxes near the interaction region in collider facilities, the radiation hardness of diamond should allow diamond detectors to function indefinitely under the same conditions. This fact alone makes diamond a very desirable detector material. Experiments are currently being performed in hopes of determining exactly to what level diamond shows radiation hardness.

Additionally, diamond is characterized by

- a low dielectric constant;
- rugged material properties;
- good electrical insulation; and
- good thermal conductivity.

[1] The term "mean path length" is somewhat confusing in that it refers to the mean of an exponential distribution, an average over electrons and holes, and an average of spatial variation of the local mean path length over the thickness of the detector. Because of the possibility for confusion, the term "mean path length" will only be used when the context makes the meaning clear. In all other cases, the terms to be used are the "local mean path length" (local referring to the value at a given position in the detector) and the "average mean path length" (average referring to the average of the local mean path length over the thickness of the detector. Both terms will always refer to the mean of the exponential distribution, and the average over electrons and holes, since $\lambda_e = \lambda_h$ by assumption. In formulae, the average over thickness will be represented by $<\lambda_q>$.

All of these properities suggest that diamond would make a good material from which to build a detector.

1.5 Goals for diamond

The ultimate goal is to create a detector with resolution capabilities comparable to those of silicon, currently the best detector available, but with better bulk properties. It is hoped that diamond will fulfill this role. A computer model of vertex detectors can make predictions which give many clues as to how close diamond can approach silicon in position resolution. Upon developing a model which can explain observed phenomena in diamond and silicon detectors, the primary problems which the model investigates and hopes to make predictions about for future improvement of diamond include:

- a small signal to noise ratio (S/N);
- poor spatial resolution;
- poor event cluster finding efficiency.

The above diamond characteristics constitute the main challenges in making usable diamond detectors for high energy physics experiments. However, work being done in the RD42 collaboration at CERN aims to increase the current understanding of diamond so that improvements can be made in the hopes that future experiments could utilize diamond technology for charged particle tracking near the interaction region.

2 Computer model of signal generation

A complete model of detectors must meet certain criteria in order to be believable. One of these criteria is that for infinite charge carrier mean path lengths, the *total* signal seen on the readout must equal the total deposited charge (given as the number of electron-hole pairs created). Another characteristic seen in data which must be found in a good model is a prediction of a non-zero signal for any non-zero mean path length, in the limit of an infinite electrode. The near-infinite electrode approximation is used in modelling dot detectors, which are essentially parallel plate capacitors with diamond between the two plates. The first attempt at modelling detectors based on the classic image charge problem of electrostatics failed this second requirement, ultimately leading to its rejection despite its apparent predictive powers. On the other hand, the current model, based on the weighting field method described by Radeka[3], is not only able to make seemingly correct predictions, but is also able to meet both of the above mentioned criteria.

2.1 The weighting field method

The weighting field method utilizes work-energy consideration to make predictions for the charge seen on the readout based on the movement of charges inside the bulk of the material.

2.1.1 Dot detectors

To understand the weighting field method, it is instructive to first consider the case of a dot detector which, to first approximation, is like an ideal parallel plate capacitor. For this case, we have the formula

$$q_i \Delta V_i = V \Delta q_i \tag{1}$$

relates the work done by the total potential difference, V, in moving the i^{th} electron or hole through a potential difference ΔV to the signal Δq which must then appear on the electrodes in order to maintain the potential difference between the two plates. Reorganizing the terms in this equation,

$$\Delta q_i = q_i \frac{\Delta V_i}{V} \equiv q_i \Delta V_i^w \tag{2}$$

obtains, where V^w represents the weighting potential, a potential normalized to unity. For this arrangement, V^w increases linearly from 0 on one electrode to 1 on the opposite electrode. Therefore, in order to find the signal induced in a dot detector, one must simply determine how far every electron and hole moves before stopping and then sum over all the charges under consideration since $\Delta V_i^w = \Delta z_i / t$ for a parallel plate capacitor, where z is the distance into the detector, and t is the thickness of the detector.

2.1.2 Strip detectors

For vertex, or strip, detectors the weighting field method becomes more complicated. As in the case of a dot detector, a potential is applied between one side of the detector and the other in order to sweep electrons and holes towards opposite electrodes to obtain a signal. However, as its name indicates, one of the electrodes is in fact divided into many strips. Every one of these electrically isolated strips is connected to its own amplifier circuit.

As in the case of dots, our goal is to find the work done by each strip in moving the charge through a given potential difference. In order to use the weighting field method for strip detectors, one must take into account the arbitrary nature of the zero point of electric potential as well as the principle of superposition which dictates that electric potentials add linearly. With the arbitrary nature of the zero point of potential in mind, the detector arrangement may be visualized as being reversed, in the sense that the solid electrode is held at ground and the strips are being held at unit potential. Because the fields add linearly, the field from an arrangement where a single strip is held at unit potential, and all the other strips and the solid electrode

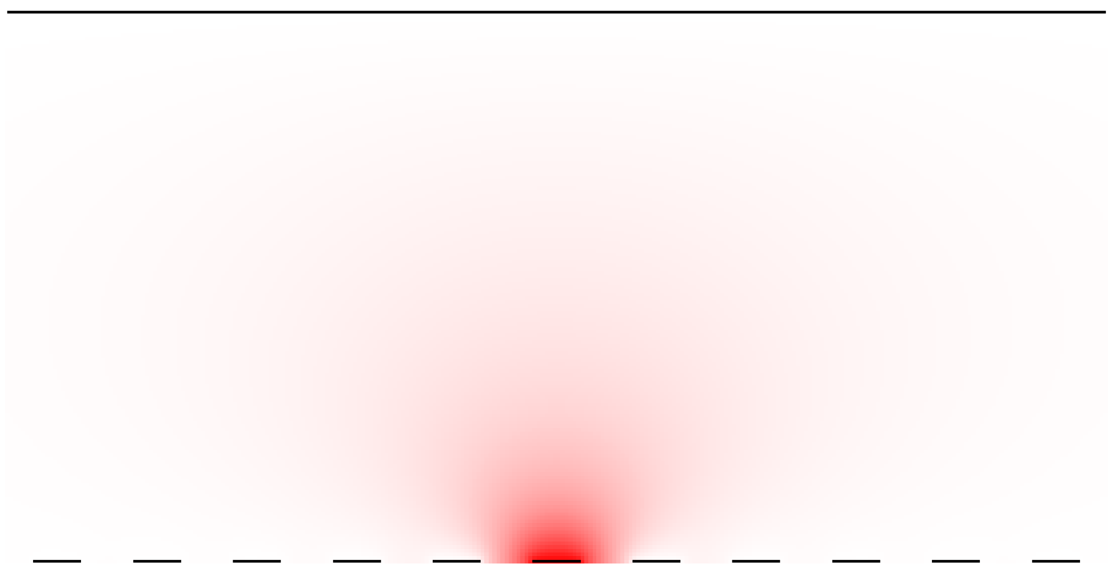

Figure 1: The weighting potential for a 300 μm thick detector. The dark line segments at the bottom of the plot represent the locations of the strips. The central strip is held at unit potential. All other strips are at ground. The solid line at the top of the plot represents the solid electrode, also held at ground.

are held at ground may be calculated instead. The field calculated in this way is the strip detector's weighting field for the strip held at unit potential. Furthermore, the applied field is then the superposition of the weighting field for all the strips in the detector. By calculating the potential due to one strip, the charge induced on that strip by the movement of charge through the *applied* field can be found by the exact same method described above. For the j^{th} strip, and the i^{th} charge, Equation 2 becomes

$$\Delta q_{i,j} = q_i \Delta V_i^{w,j} \quad . \tag{3}$$

Despite the simplicity of Equation 3, calculation of the weighting field for the geometry described is non-trivial. Because of the complicated geometry involved, the numerical method of relaxation on a 1 μm grid[4] was used. Given a reasonable first guess at what the electric potential looks like inside the detector, the relaxation method will find the exact field by simultaneously satisfying Laplace's equation, $\nabla^2 V = 0$, in its finite difference form for all points on the grid. Though reasonably accurate, this method is very inefficient for large grids. This fact has caused considerable difficulty in trying to model thicker detectors. Appendix A describes the method used for obtaining a reasonable first approximation of the electric field using the method of separation of variables and a Fourier series.

Figure 1 shows the calculated weighting potential for a 300 μm thick detector with strip pitch equal to 50 μm and a strip width of 25 μm. In order to test if this represents the "correct" field, this field is superimposed upon itself shifted by integral multiples

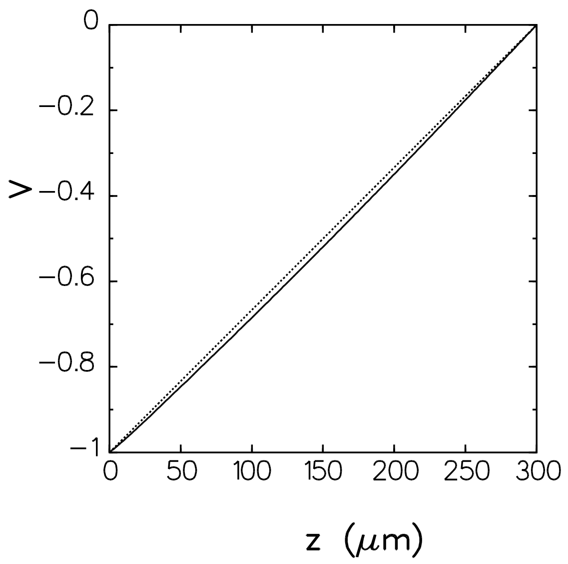

Figure 2: V_{superpos} as a function of depth into the detector for the 300 μm detector. The dotted line is the linear rise expected in the limit of a parallel plate capacitor.

of 50 μm, the strip pitch. This is equivalent to looking at the potential that would arise if all strips were held at unit potential, for which a field closely resembling that of a parallel plate capacitor is expected. Figure 2 shows the potential as a function of depth through the detector above the central strip after this superposition. The fact that the potential increases nearly linearly from -1 to 0 indicates that we have come very close to finding the correct weighting potential. The fact that our weighting potential starts at -1 instead of $+1$ reflects an arbitrary sign convention used in the circuits to obtain positive signals.

2.2 Charge deposition, movement, and diffusion

In order to completely model CVD diamond detectors electron and hole deposition, movement, and thermal diffusion must be taken into account. Some approximations in dealing with these phenomena simplify calculations, while others are necessary due to incomplete understanding of what is happening inside of the detectors.

2.2.1 Electron hole deposition

In a real detector, a high energy charged particle passes through the diamond and loses a fraction of its initial energy to ionization of the detector material. This ionization appears as an array of free electrons and holes in the material. For diamond, 13 eV is required to create one electron-hole pair. For a minimum ionizing charged π meson used in beam tests, full analysis of the charge loss reveals an average charge deposition

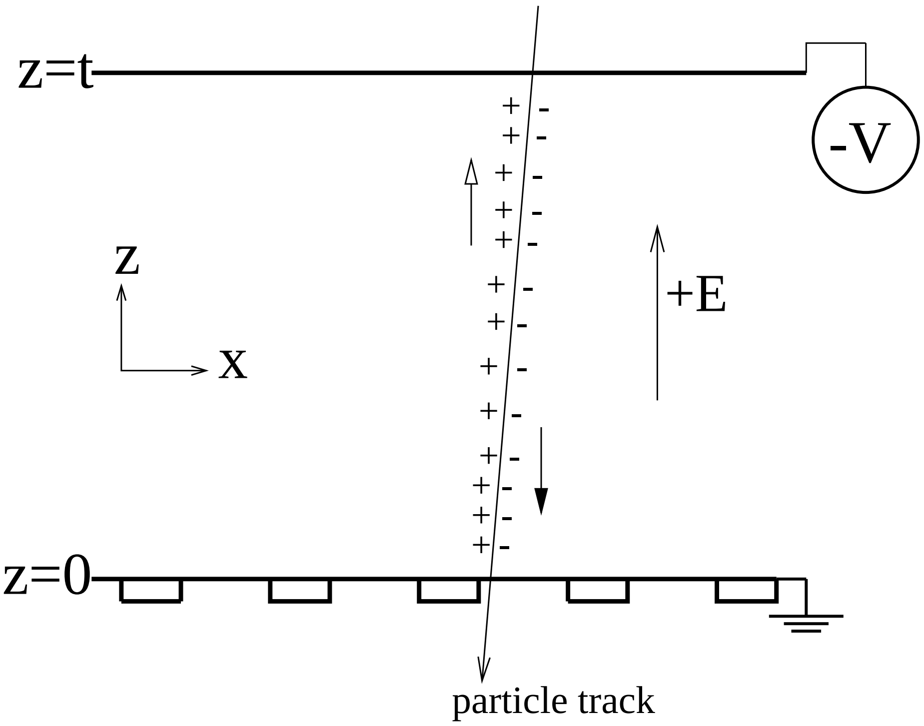

Figure 3: Illustration of charge deposition in a strip detector. Some of the conventions of the model are also shown here. Note, however, that the model assumes that the track is in fact perpendicular to the strip plane.

of 3600 electron-hole pairs per 100 μm of diamond[5]. This value is the mean of a Landau distribution. The model uses the experimentally determined distribution as input instead of a true Landau. Although it is believed that non-uniformity in the charge deposition throughout the depth of the detector may be important for thicker detectors, the model currently assumes uniformity in order to simplify calculations for the thinner detectors. Figure 3 is an illustration of a strip detector and charge deposition.

2.2.2 Electron and hole movement

Under the influence of an applied electric field, electrons and holes drift from their point of liberation towards opposite electrodes. However, when an external field is applied, only the potential value at the two electrodes is known with certainty. Internal polarization of the diamond due to charge build up could give rise to a non-constant field inside the bulk of the diamond. However, because of difficulties in measuring the true nature of this field, uniformity throughout the detector thickness is assumed.

There are several quantities which quantify how fast and how far an electron or hole will move in the bulk before coming to rest. The mobility quantifies how fast an electron or hole will move per unit electric field in a given material. For diamond we take $\mu_e = 1800$ cm$^2/Vs$ and $\mu_h = 1200$ cm$^2/Vs$ for the mobility of electrons and holes respectively[5].

The mean path length, a function of the charge carrier lifetime, determines how far the charge will travel, on average, before becoming trapped and having its movement stopped. In order to model this phenomenon, a time slice approach to charge movement is utilized. For each slice of time, Δt, the local mean path length of each electron and hole determines its probability to continue moving during that time slice. If the charge is still flagged as moving, it moves an absolute distance $|E|\mu\Delta t$ in that time slice. This process is repeated until all the charges have come to rest.

For a detector arrangement which has a local mean path length, λ_q, equal to zero on one side and an average mean path length of $<\lambda_q>$, it is assumed that λ_q varies linearly from 0 to $2<\lambda_q>$ in going from one side to the other[2]. Furthermore, it is assumed that electrons and holes have the same local and average mean path lengths.

2.2.3 Diffusion of charge

In addition to the movement of charge along the electric field, electrons and holes will also diffuse laterally. This amount of diffusion is given by the Einstein relationship[6]:

$$P_{e,h}(x, \Delta t) = N \exp \frac{-qx^2}{4\mu_{e,h} k_B T \Delta t} \quad . \tag{4}$$

For each time slice, Δt, a charge is moved laterally according to a Gaussian distribution with a width as prescribed by the above equation. This model assumes the detector is operated at room temperature, T.

3 Modelling the X^* detector

In order to make comparisons between the predictions of the model and the test beam data, both the inherent diamond characteristics and the operational parameters must be taken into account. The characteristics of diamond which are included in the model are

- the average mean path length, $<\lambda_q>$;
- a guess as to how λ_q varies through the thickness of the detector;
- the strip width and pitch; and
- the thickness of the diamond.

The operational parameters which are included are

- the applied voltage between the solid electrode and the strips;
- the average noise on strips;

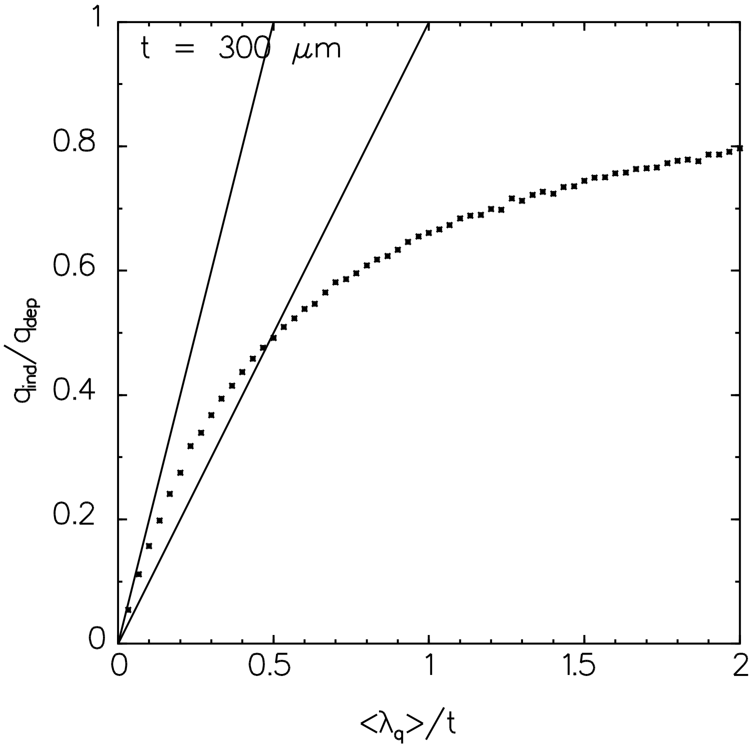

Figure 4: Ratio of induced charge to deposited charge as a function of the ratio of collection distance to thickness for a dot. To make this plot, it was assumed that collection distance varied between 0 and $2\lambda_q$ from one side of the detector to the other. The straight lines represents the incorrect assumptions $q_{\rm ind}/q_{\rm dep} =< \lambda_q > /t$ and $= 2 < \lambda_q > /t$.

- digitization of the amplifier;
- pedestal addition and subtraction;
- whether the strips are on the high or low λ_q side; and
- the conversion factor between number of electrons and number of ADC counts.

3.1 Characteristics of the X^* detector

The 300 μm thick X detector in its pumped state, represented by X^*, posesses mean path lengths which are assumed, as described above, to vary linearly from 0 μm on one side to $2 < \lambda_q >$ on the opposite side. Using the information from Figure 4, in conjunction with an experimentally determined 5-strip pulse height distribution and the conversion factor between electrons to ADC counts, a best estimate of 37.5 μm obtains for the X^* mean path length. Determination of this number relies on the fact that a minimum ionizing particle deposits an average of 3600 electron hole pairs per 100 μm of diamond traversed. The strip pitch for X^* is 50 μm and the strip width is about 25 μm.

It is interesting to observe the non-linear rise seen in Figure 4. This curve, however, appears to be universal for all detectors where λ_q varies from 0 to $2 <\lambda_q>$, and the fact that it is non-linear appears to be completely independent of the spatial variation of λ_q. Although the Figure 4 shows a line for $q_{\text{ind}}/q_{\text{dep}} = \lambda_q/t$, one might actually expect that the right hand side of the equation should be $2\lambda_q/t$, since $\lambda_q = \lambda_e = \lambda h$ and the mean distance of separation between electrons and holes should be something like $\lambda_e + \lambda_h$. However, because the electrons and holes cannot always travel as far as they would in an infinitely thick detector (because they hit the electrodes), the rise is in fact slower than $2\lambda_q/t$.

3.2 Strips on the growth side of X^*

The growth side of a detector, with the larger average crystal size, is generally the side with greater collection distance. As previously indicated, the model treats a detector with strips on the growth side as having a local mean path length which decreases linearly from $2 <\lambda_q>$ to 0, or 75 μm on the strip side to 0 μm on the solid electrode side in the case of X^*. Electrons move towards the strips, while holes move towards the solid electrode. As will become clearer later, the fact that the mean path length vanishes at the solid electrode side gives rise to many very interesting phenomena seen both in the model and the data.

3.2.1 Input and output charge distributions

The experimentally determined distribution of 5-strip pulse heights for strips on the substrate side, once converted from ADC counts to electrons, serves as the parent distribution of charge deposition in the detector. From this distribution, approximately 8 percent of events were taken. Due to the work-energy considerations given in Equation 1, the total integrated (over all strips) pulse height is expected to be independent of which side the strips are on. As shown in Figure 16, the mean of the parent distribution is 75.1 ADC counts. Figure 5 and Figure 6 show the 3- and 5-strip pulse heights, respectively, as predicted by the model along side the same distributions for the X detector at different stages of pumping, for strips on the growth side. The experimental distributions of interest are those labeled as X^*. The model predicts only a slightly larger mean in both cases, which would seem to indicate that the approximation of $<\lambda_q>$ is reasonably accurate.

3.2.2 Gross features of signal generation in typical events

Before examining more detailed comparisons between the two detectors, it is both interesting and instructive to compare a few typical strip responses to a track. Figure 7 shows the pulse heights on the 5 strips to either side of a track. For the data displays, the arrow indicates the location of the particle's trajectory projected into the plane of

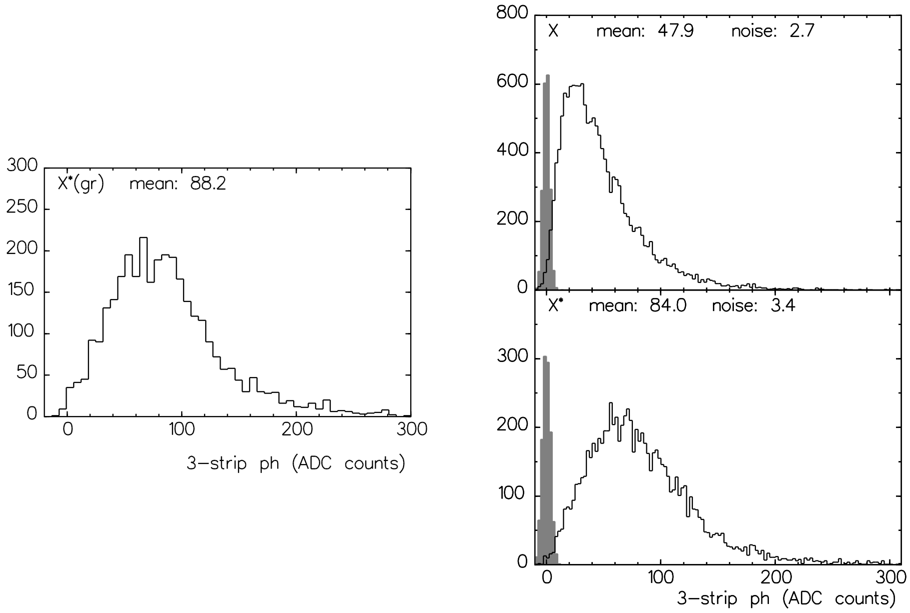

Figure 5: 3-strip pulse heights as predicted by the model (left) and as found experimentally (right) for strips on the growth side of the X detector. The extra darkened histogram in the data plot is the distribution of noise in the detector.

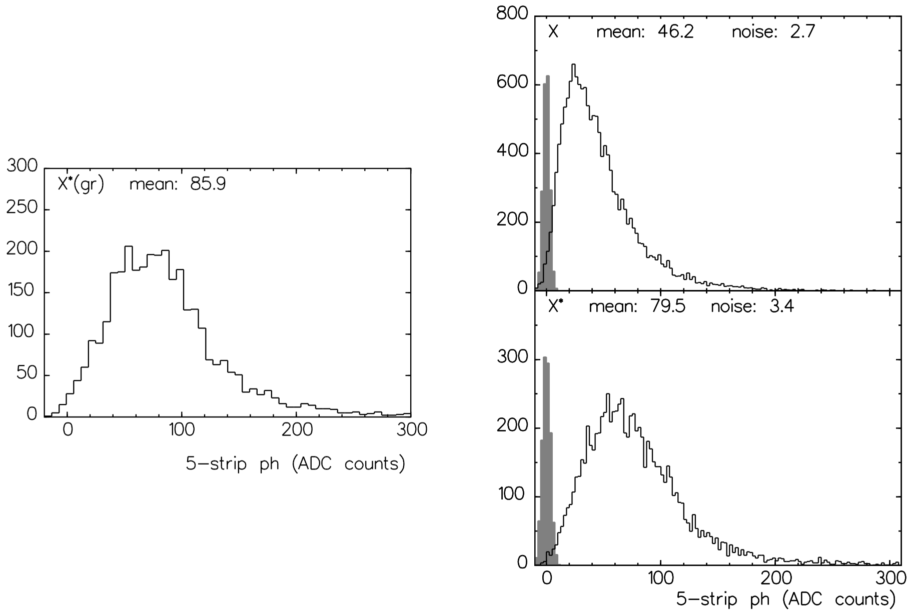

Figure 6: 5-strip pulse heights as predicted by the model (left) and as found experimentally (right) for strips on the growth side of the X detector.

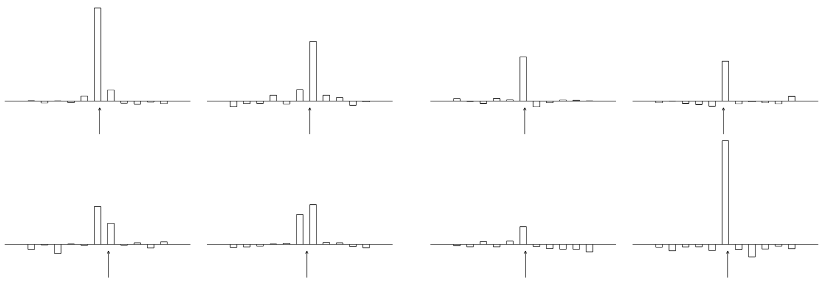

Figure 7: Some typical strip responses for strips on the growth side of the X detector. Model events are on the left, data events are on the right. The arrow represents the projected track location. Please note that both sets of plots were picked randomly and independently, so there is not supposed to be any direct correlation between any one plot from the model and another from the data. It is only the general likeness which is being shown.

the diamond. For the model displays, the arrow represents the location of the initial electron-hole array added to a 5 μm Gaussian error, in an attempt to simulate the track projection error of the data.

The most distinguishing features to note in these event displays for strips on the growth side are the large pulse heights on strips in immediate proximity to the track location, and negative pulses on the strips farther away from the track location. An understanding of these negative signals comes from an examination of the weighting field and the formulas used to calculate the final signal seen on a given strip.

Expanding Equation 3 for one electron-hole pair (which is reasonable to do, since for every electron liberated in the material, there will be an associated hole created), the formula for the charge on the j^{th} strip becomes

$$\Delta q_j = q_e(V_{e_f}^{w,j} - V_{e_i}^{w,j}) + q_h(V_{h_f}^{w,j} - V_{h_i}^{w,j}) \tag{5}$$

where q_e and q_h represent the charge on an electron and hole, respectively, and f and i refer to the final and initial locations of the charges, respectively. Understanding the origin of negative signals comes from using two facts: the charge on a hole is equal and opposite to the charge on an electron and, because the electron and hole are created as a pair at the same location in the bulk of the material, $V_{h_i}^w = V_{e_i}^w$. The remaining terms from Equation 5 become

$$\Delta q_j = q_e(V_{e_f}^{w,j} - V_{h_f}^{w,j}) \quad . \tag{6}$$

Because the mean path length goes to zero at the solid electrode side and no holes reach the solid electrode, the last term in Equation 6 is necessarily non-zero for all holes because the weighting field does not equal zero anywhere in the bulk of the diamond. Because they are moving towards a region of greater mean path length, the majority of electrons will reach the strip side of the detector. If it is assumed that the electron under consideration is in this majority group and that it hits a strip, then the first potential term on the right hand side of Equation 6 becomes unity for the strip which the electron hits, and becomes zero for all other strips. If the electron hits in between two strips, the potential term will be some number greater than zero and less than one for all strips. On average, therefore, for *all* electron-hole pairs, there will be a large positive contribution on the central strip(s) from the electrons which hit those strips, surrounded by negative signals from the far away holes (small negative signal) and the zero (or small positive) contribution from electrons on all the neighboring strips.

Although this way of analyzing the problem makes the understanding a bit easier, it is not really the most accurate description of the charge induction. It is more accurate to examine what happens as each individual charge moves through a weighting potential difference, ΔV^w. For the purposes of discussion, consider a weighting field which varies between zero and +1, and a charge on the electron of +1. From Equation 5, it is clear that if the electron moves in such a way that $V_f^w < V_i^w$, which it can do for a strip *not* directly below its physical location (see Figure 1 away from the center), then it will induce a negative signal on that strip whose weighting field is being considered. Similarly, if the electron moves in such a way that $V_f^w > V_i^w$, as it will do anywhere for the strip above which it is located or when near the solid electrode for all strips, then it will induce a positive charge on those strips. Because $q_h = -q_e$, the argument is exactly reversed for holes. Thus, both electrons and holes are able to induce either a positive or negative signal on any given strip (provided it is not the central one) – the sign that arises being due to the location of the charge in the bulk of the material.

3.2.3 The strip response function for $X^*(\mathbf{gr})$

In order to eliminate, in some sense, the noise variations evidenced in Figure 7 showing a few typical events, a strip response function plot averages this type of display over all events. Figure 8 shows the average pulse height on a strip as a function of the distance from that strip to the track location. Δx in these plots represents the distance from the center of a strip to the track location, in units of strips. In the experimentally derived plot the track position is extrapolated from the particle trajectory fit made from the silicon planes in the detector telescope. For the model plot the track location is taken to be the location in the x direction in which the initial array of electrons and holes was placed, to which a 5 μm Gaussian random variable has been added in order to simulate the track extrapolation error.

The model and the data agree both qualitatively and quantitatively, in both the large positive central pulse height and in the surrounding negative tails. Figure 9 shows the negative tails in greater detail. Again, the plots reveal good agreement between the model and the data. However, the model shows more prominent "bumps and wiggles" than does the data. The peaks of these bumps occur at approximately the half integers. As discussed above, these are believed to occur because of the non-vanishing weighting field between strips, which gives rise to a closer cancellation between the holes which remain in the bulk far away, and the electrons which do not physically hit a strip.

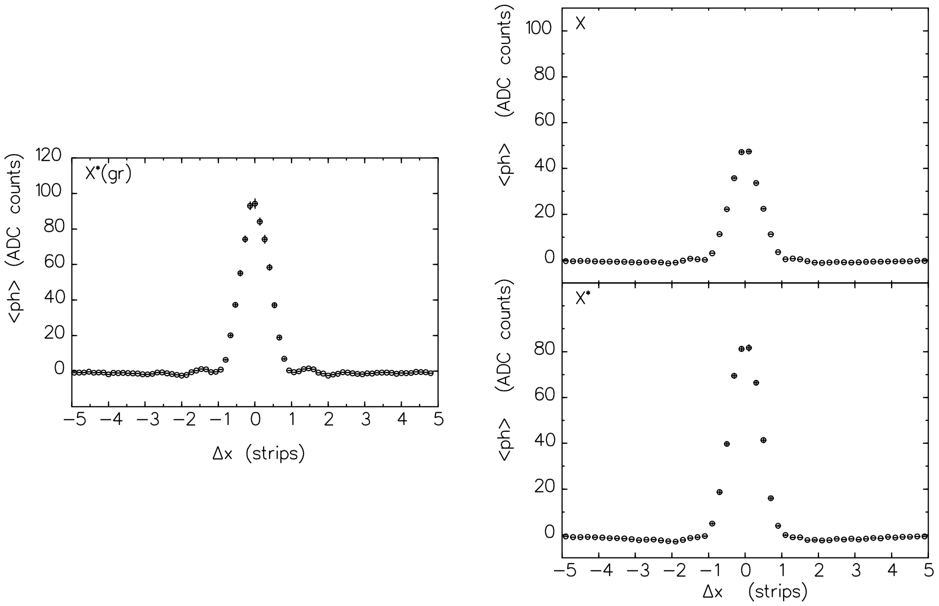

Figure 8: Strip response function for strips on the growth side of X^*. Model predictions are on the left, experimental results for X at various stages of pumping are shown on the right. The model attempts to simulate X at the X^* stage of pumping.

There are many possible explanations for why these feature are much more prominent in the model than in the data. One such explanation is the fact that, according to the model, when an electron hits the strip side of the detector, it just stops moving, and can induce the positive signal on all strips. However, the more likely case is that the electron hits the interstrip region and subsequently drifts laterally to be collected by the closest strip. When this happens, the electron will induce its full signal on that strip, but *no* signal on any other strips. The more prominent features in the model may also be due to an error in the calculation of the weighting field made by assuming the diamond to be vacuum rather than dielectric.

3.2.4 Charge loss between strips

One question which naturally arises in considering the signal generation in any strip detector is whether or not there is any signal loss between strips. Examination of the average 3- or 5-strip pulse height as a function of track location illuminates the answer to this question. The 3- and 5-strip pulse heights are transparent quantities, meaning that their value may be found for every event, whether or not event-finding algorithms show a hit in the diamond. Instead of plotting the 3- or 5-strip pulse heights purely as a function of position along the detector, an examination is made of the pulse heights as a function of s_{track}. The fractional part of the track position in strip units, s_{track}, is zero if the track goes directly through the center of a strip, and

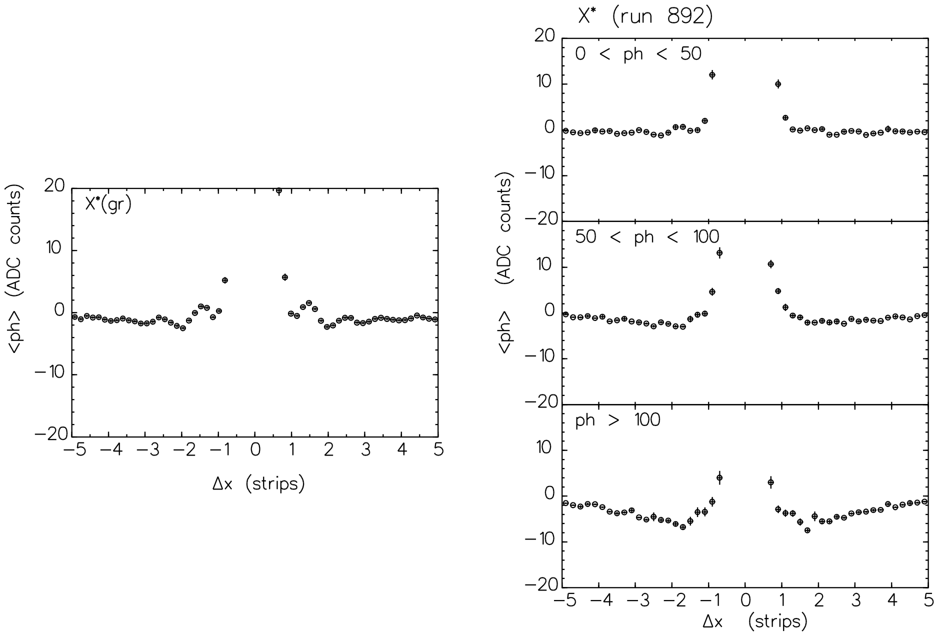

Figure 9: Strip response function for strips on the growth side of X^* showing in detail the negative going tails of the distribution. Model predictions are on the left, experimental results for X for different ranges of central pulse height are shown on the right.

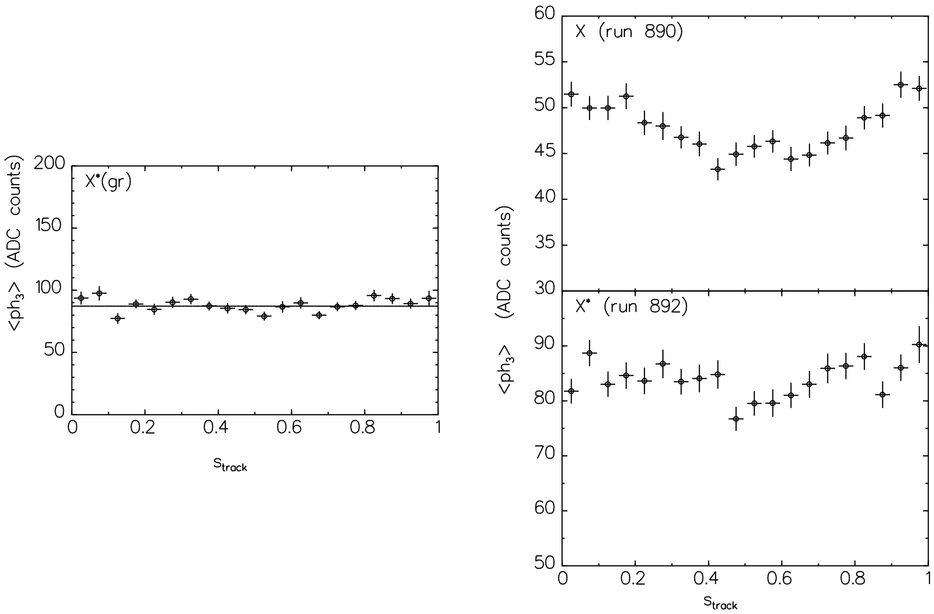

Figure 10: Mean 3-strip pulse height as a function of the fractional part of the track position in strip units with strips on the growth side of the X detector for the model (left, with a line to guide the eye) and the data (right).

is one if the track goes through the center of the next strip to the right. The folding over is done to give better statistics, and to make the plot easier to read. Figure 10 and Figure 11 show the model's predictions and the experimental plots of average 3- and 5-strip pulse heights as a function of this folded over track position. Within error bars, it appears as though the model predicts no charge loss between strips. This phenomenon is expected from the work-energy relationship, which suggests that *something* must always be doing the work to move the charges, independent of the charges' final locations. It is clear that there *is* a definite dip seen in the data for the X^* detector with strips on the growth side. The reason for this discrepancy is not understood, but incorrect modelling of charge transport in the interstrip region is suspected to possibly play a role.

3.2.5 Position resolution – cluster analysis

The quantity of ultimate interest in making viable diamond particle detectors is the spatial resolution. Silicon, with a reported position resolution of 3-4 μm[7], leads the solid state particle detector field in position resolution. Measurement of the resolution of the detector necessitates a cluster analysis.

For a cluster analysis to find a track, the first requirement is that there be at least one strip in the diamond with a signal greater than 3 times the rms of the noise. The strip with the maximum pulse height meeting this criterion becomes the seed strip for

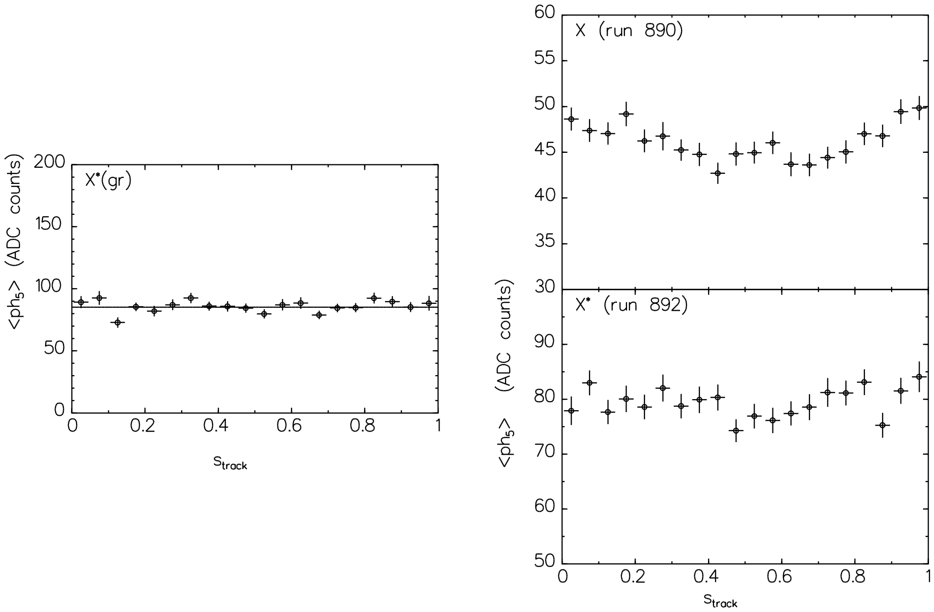

Figure 11: Mean 5-strip pulse height as a function of the fractional part of the track position with strips on the growth side of the X detector for the model (left, with a line to guide the eye) and the data (right).

building a cluster. A cluster is then built by adding neighboring strips whose pulse height is greater than 2 times the noise rms. Figure 12 shows the mean number of strips in a cluster as a function of the folded over track position. It should be noted that a point will enter this plot if and only if a cluster is found – in other words, only if the number of strips in the cluster is greater than or equal to one. The model and the data show about a 96% cluster-finding efficiency when strips are on the growth side. The total amount of charge diffusion, governed by Equation 4, is on the order of approximately 10 μm. With strips on the growth side, diffusion is the primary source of charge spreading. Thus the rise from 1 to 2, as $s_{\rm track}$ nears 0.5 is expected, since it is only when the track goes between strips that electrons would be expected to be collected on more than a single strip.

To determine the resolution of the detector, calculation of the difference between the extrapolated track position and the cluster hit position is necessary. For a cluster of n strips, the formula

$$u_{\rm hit} = \frac{\sum_{i=1}^{n} x_i \; q_i}{\sum_{i=1}^{n} q_i} \tag{7}$$

determines the cluster hit position, where x_i is the location of the center of the i^{th} strip. The residual of the track, Δu, defined by $\Delta u = u_{\rm hit} - u_{\rm track}$, measures the error in the cluster position finding algorithm. This error is expected to be a function both of the signal to noise ratio and of the amount of spreading of the signal (i.e.–how many strips are in the cluster.) Figure 13 shows the hit residual versus the folded

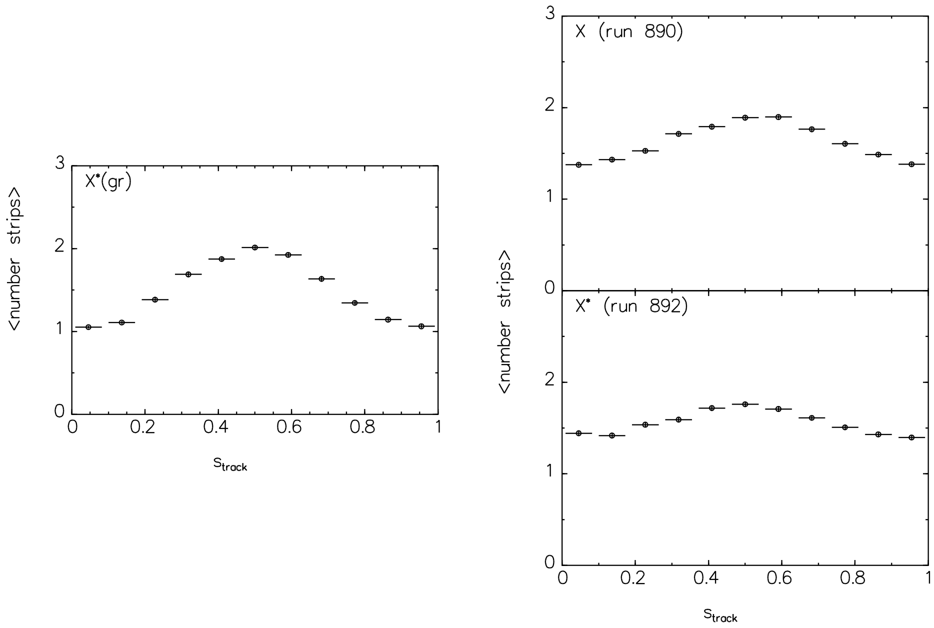

Figure 12: Mean number of strips in a cluster as a function of the fractional part of the track position as predicted by the model (left) and data (right) for strips on the growth side of X.

over track position. The prominent streaks in this plot correspond to single strip clusters.

The resolution of the detector is given by the root mean square deviation from zero of the residual for all events. Figure 14 is a historgram of all the residuals along with a Gaussian fit and the best estimate of the width of the Gaussian. The information contained in these plots is a mixture of the "intrinsic resolution" of the detector and the track projection error. Therefore, the fact that the model predicts a better resolution than the data show may be due to an underestimate of the track projection error. Although channel-to-channel gain variations in the amplifier also make the resolution slightly worse, it does not appear as though this effect would be significant enough to account for the difference seen[8].

3.3 Strips on the substrate side

The substrate side of a detector generally exhibits a smaller local mean path length than the growth side. Although microcrystal size may have something to do with this fact, the exact reason is not known. For X^* the spatial variation in the local mean path length with strips on the substrate side is modelled as increasing linearly from 0 μm on the strip side to $2 < \lambda_q >$, or 75 μm on the solid electrode side. As when strips are on the growth side, electrons move toward the strips and holes move toward the solid electrode. The fact that the mean path length vanishes at the readout on

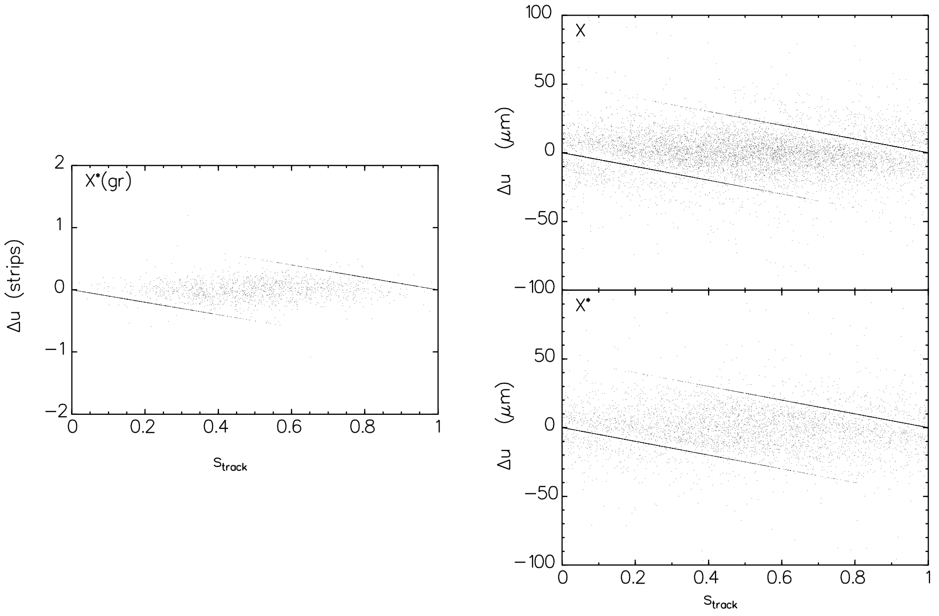

Figure 13: Difference between cluster position and track position as a function of the fractional part of track position for the model (left) and the data (right) for strips on the growth side of X.

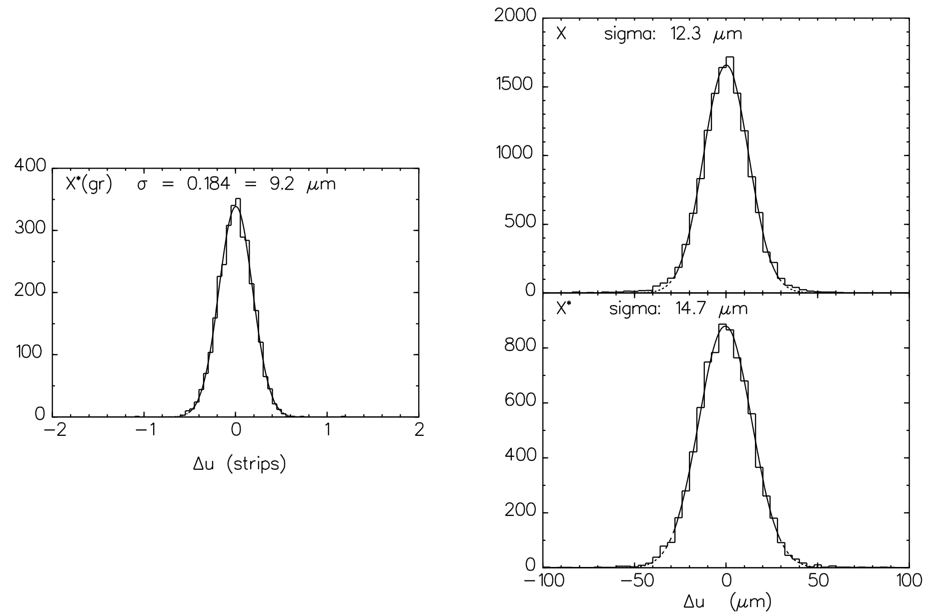

Figure 14: The resolution as predicted by the model (left) and according to the data (right) for X with strips on the growth side.

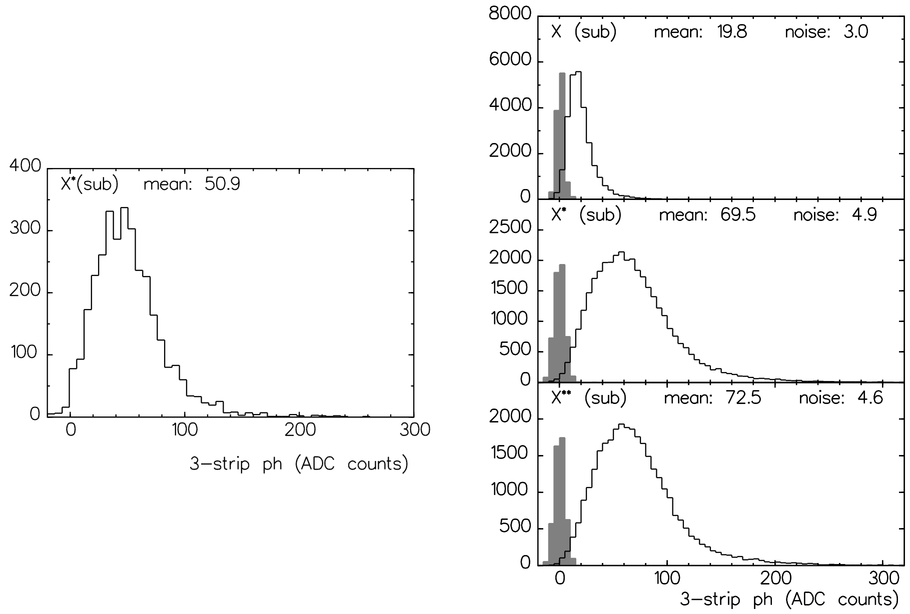

Figure 15: 3-strip pulse heights as predicted by the model (left) and as found experimentally (right) for strips on the substrate side of the X detector.

the strips means that no charge is physically collected on any strips. The importance of this fact will become clear in the discussion that follows.

3.3.1 Input and output charge distributions

From the 5-strip pulse height distribution for strips on the substrate side parent distribution, approximately 8 percent of events were taken. Again, due to the work-energy considerations given in Equation 1, the total pulse height, integrated over all strips, is expected to be independent of which side the strips are on. Figure 15 and Figure 16 show the 3- and 5-strip pulse heights respectively, as predicted by the model along side the same distributions for the X detector at various stages of pumping with strips on the substrate side. The experimental distributions of interest are those labeled as X^*. Where the model for strips on the growth side predicted larger than expected pulse heights, the model predicts a mean which is too small when strips are on the substrate side. The reason for this effect is not understood. However, it is possible that this effect results from starting out with the experimental distribution, instead of a theoretical Landau, as the input charge deposition distribution. The convolution of this distribution with the spatially varying exponential path length distribution may be responsible for the lowering of the mean value seen in the model.

3.3.2 Gross features of signal generation in typical events

In looking at Figure 17 it is obvious that putting strips on the substrate side differs

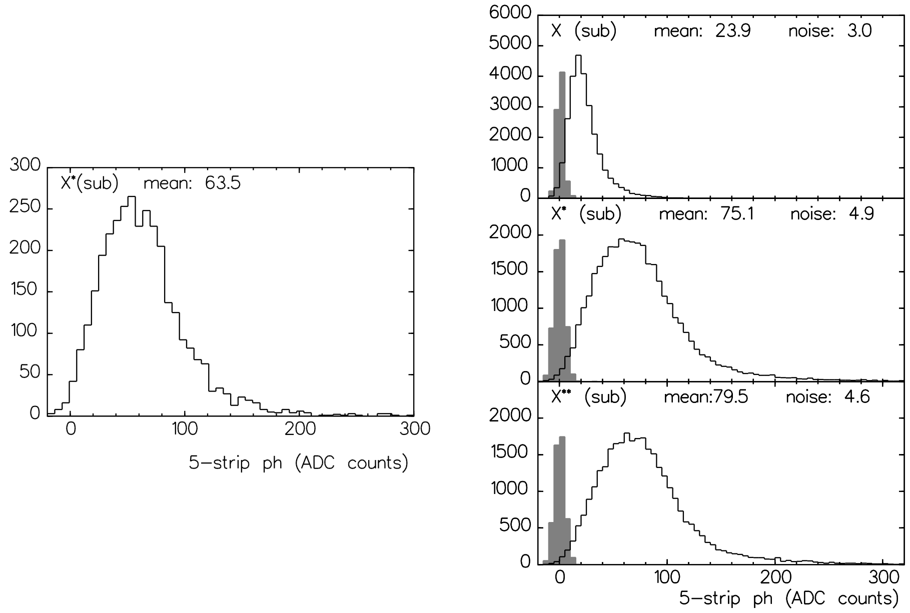

Figure 16: 5-strip pulse heights as predicted by the model (left) and as found experimentally (right) for strips on the substrate side of the detector.

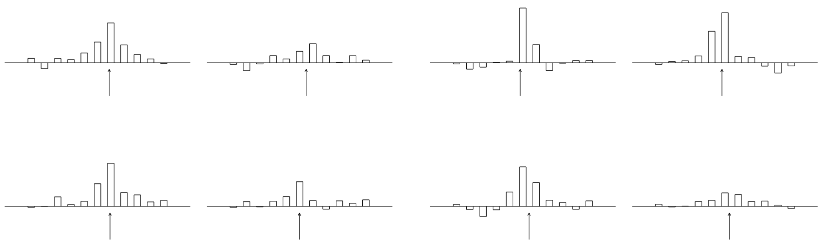

Figure 17: Some typical strip responses for strips on the substrate side of X. Model events are on the left, data events are on the right. The arrow represents the projected track location. Please note that both sets of plots were picked randomly and independently, so there is not supposed to be any direct correlation between any one plot from the model and another from the data. It is only the general likeness which is being shown.

greatly from putting strips on the growth side (see Figure 7.) With strips on the substrate side, shallow, wide distributions arise, as opposed to the large, narrow distributions characteristic of strips on the growth side. Additionally, the negative going pulses on strips around the centroid which were prominent features in the growth side distributions are absent on the substrate side.

An explanation for these different features again comes from analysis of Equation 6 for the charge induction from a single electron-hole pair. The most important fact to remember for this analysis is that the mean path length is *zero* at the strip side of the detector. This means that *no charge will be physically collected on the strips.* The electrons moving towards the strips will, on average, remain in the bulk of the diamond near the strips. The holes, on the other hand, will move away from the strips, and the majority will hit the solid electrode.

For this typical final state, Equation 6 becomes $\Delta q_j = q_e(V^{w,j}_{e_f} - 0)$ which is positive definite given the sign convention of the problem ($q_e = -1$ and $-1 \leq V^w \leq 0$). Because this equation holds for the typical electron-hole pair, it stands to reason that the signal, before addition of noise, will always be positive.

The extra width in the distribution for strips on the substrate side may be attributed to the fact that charge is not collected on the strips. On the growth side, the majority of electrons will hit one or two strips upon which they will induce their full charge. These same electrons will induce nothing on neighboring strips. With strips on the substrate side, the majority of electrons remain in the bulk, where V^w remains non-zero for *all* strips. This wide positive distribution is analogous to the wide negative distribution seen with strips on the growth side. In this case, however, the electrons which remain in the bulk are closer to the strips and have the opposite sign. In some sense, the wide distribution seen is a sort of profile of the weigthing field at the average final location of the electrons. From Figure 1, one can see that this profile is significantly positive out to a distance of a few strips when that average final position is not too close to the strips.

3.3.3 The strip response function for X^*(sub)

As a way of eliminating the noise and charge deposition variations from the analysis of the strips response to a track, a strip response function plot averages over all events and track positions. Figure 18 shows the strip response function for strips on the substrate side as predicted by the model and as found by the data analysis. Both the model and data show a very wide, non-Gaussian distribution. The fact that the model predicts a shallower, wider distribution is correlated with the lower than expected 5-strip pulse height (see Figure 16) in that, with a wider distribution, a smaller percentage of charge will be collected in only 5 strips. These different characteristics may be an indication of some sort of internal polarization of the diamond which is not completely understood.

3.3.4 Charge loss between strips

Figures 19 and 20 show the 3- and 5-strip pulse height as a function of the fractional

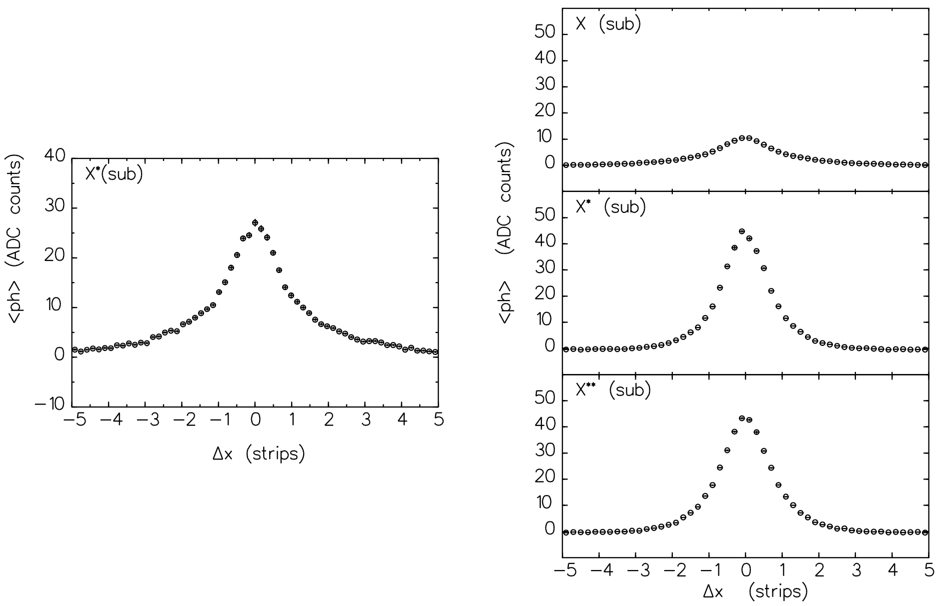

Figure 18: Strip response function for strips on the substrate side of X. Model predictions are on the left, experimental results for X at various stages of pumping are shown on the right. As in all other cases, the experimental plot of interest for comparison is the one labelled X^*.

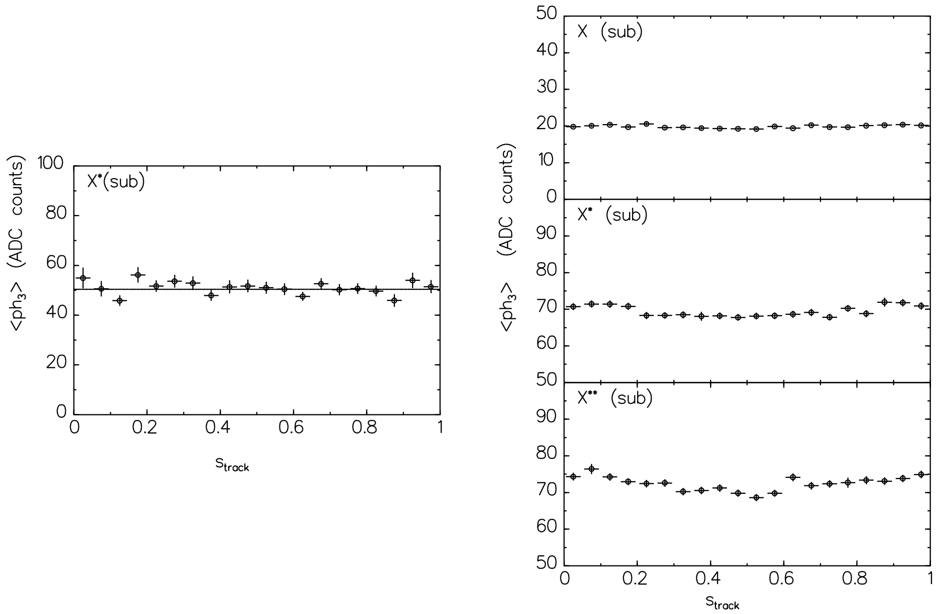

Figure 19: Mean 3-strip pulse height as a function of the fractional part of the track position strip units when strips are on the substrate side of the X detector for the model (left, with a line to guide the eye) and the data (right).

part of the track position in strip units, s_{track}. Neither the model nor the data appear to show evidence of charge loss between strips.

3.3.5 Cluster analysis for strips on the substrate side

Figure 21 shows the mean number of strips in a cluster as a function of s_{track}. When strips are on the growth side, the average number of strips in a cluster increased when the track passed close to half way between strips, as is expected because the positive part of the signal comes from the electrons which hit the strips and whose lateral spread is governed by Equation 4. The total spread is small compared to the strip pitch, so it is expected that only 1 strip or 2 strips (when the track is between strips) will show significant positive signal (see Figure 12). On the other hand, when strips are on the substrate side, the spread in signal is correlated with the width of the strip response function plot, and many strips are expected to be illuminated in each event. Thus it is not surprising that Figure 21 shows no appreciable rise at $s_{\mathrm{track}} = 0.5$. The fact that there is some rise in the experimentally derived plot is indicative of the greater central peaking seen in the strip response function of Figure 18.

The model shows a 77% efficiency for finding clusters for when strips are on the substrate side. This is much less than the 96% seen with strips on the growth side. The data show an efficiency of approximately 95% for strips on either side. The discrepancy between this number and the model number for the substrate side may

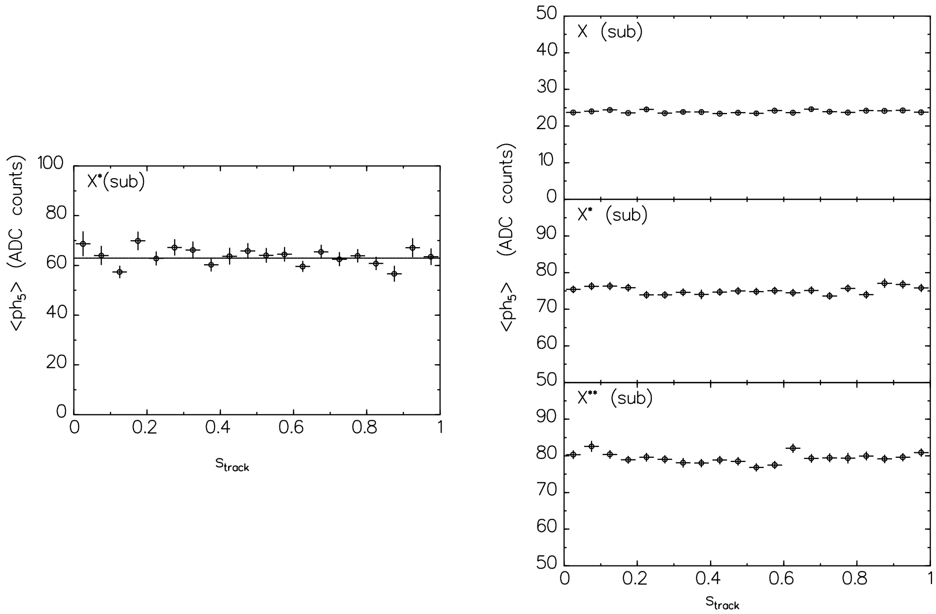

Figure 20: Mean 5-strip pulse height as a function of the fractional part of the track position in strip units for the model (left, with a line to guide the eye) and the data (right) for the X detector with strips on the substrate side.

be due to the wider strip response function seen in the model – because the signal is spread out over more strips in the model, the chances of finding a strip with a pulse height equal to 3 times the rms of the noise are much smaller.

As when strips are on the growth side, Equation 7 determines the location of the track according to the cluster analysis. The residual of the track, defined by $\Delta u = u_{\text{hit}} - u_{\text{track}}$ as a function of s_{track} for strips on the substrate side is shown in Figure 22. The features of this plot are much different from those seen in Figure 13 for strips on the growth side. There are many more events in which the residual is larger than one-half strip unit (the maximum expected for digital resolution). This can be understood from the fact that noise, added to a very wide and shallow distribution, can easily shift around the cluster's seed strip as well as the relative effect(s) of neighboring strip(s).

The resolution of the detector is given by the root mean square deviation from zero of the residual for all events. Figure 23 is a historgram of all the residuals along with a Gaussian fit and the best estimate of the width of the Gaussian. The poorer resolution predicted by the model is most likely a consequence of the wider charge spreading seen in Figure 18. Because the signal remains significantly positive out to a considerable distance, strip noise may push one or more of these strips above threshhold for inclusion in the cluster for a given event, and thus introduce an asymmetric pull of the residual in one direction or the other. Although this effect is common to both the model and the actual detector, the effect will be much more

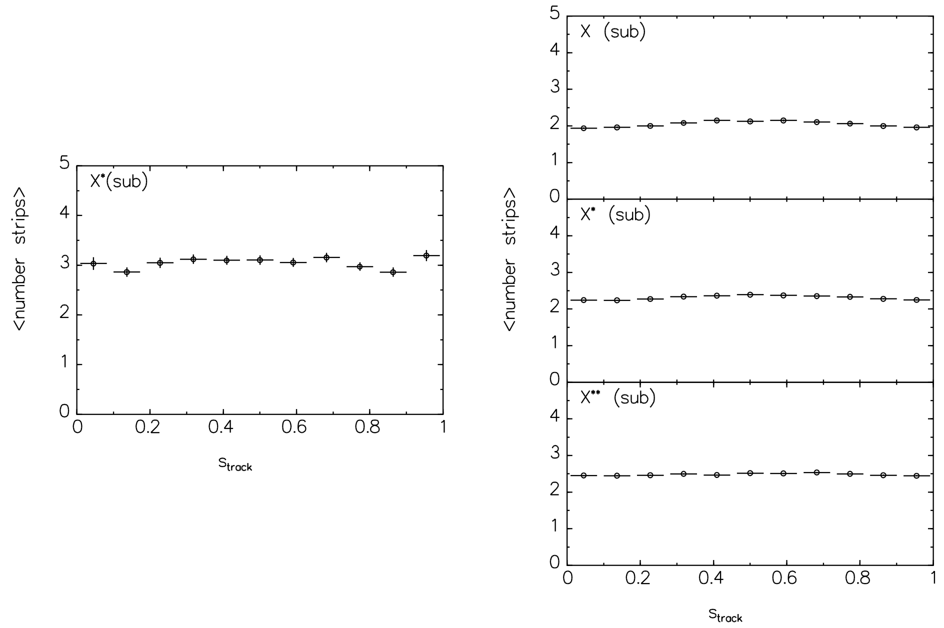

Figure 21: Mean number of strips in a cluster as a function of the folded over track position as predicted by the model (left) and the data (right) for strips on the substrate side of the X detector.

noticable in the shallower distribution of the model.

3.4 Conclusions for X

One of the most surprising results to come out of the modelling of the X detector was the fairly accurate reproduction of the various prominent features unique to operation with strips on one side as opposed to the other with very few assumptions. It was not anticipated that these differing features could be predicted from purely geometric considerations, specifically the spatial variation of the mean path length.

The most important predictions and verifications made by the model to date are:

- the explanation of the wide shape of the signal distribution with strips on the substrates side;
- the accurate prediction of much narrower central pulse height observed when strips are on the growth side;
- an explanation of the negative tails in the strip response function when strips are on the growth side;
- an indication that for wider and shallower signal distributions, efficiency will be poor;

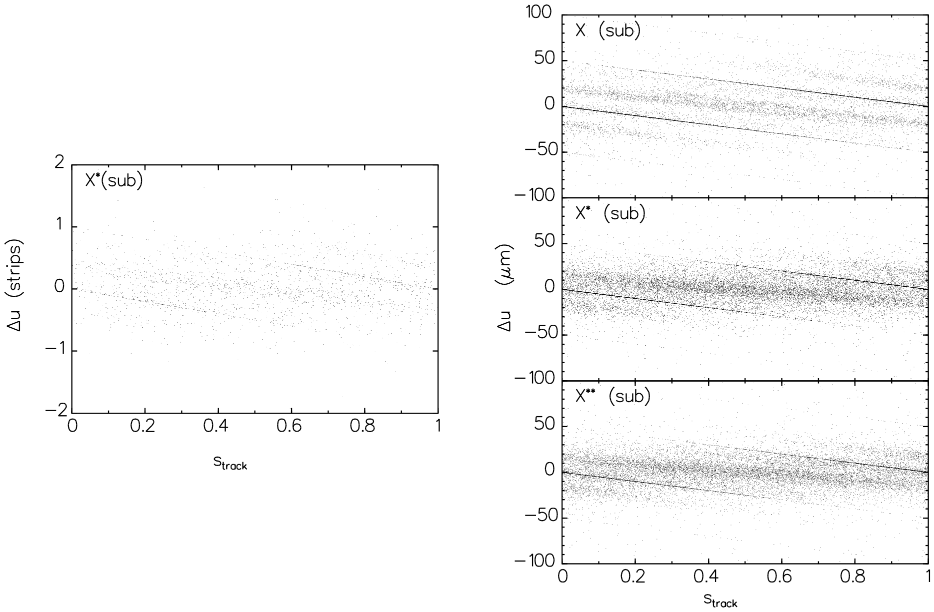

Figure 22: Difference between cluster position and track position as a function of the fractional part of the track location in strip units for the model (left) and the data (right) for strips on the substrate side of X.

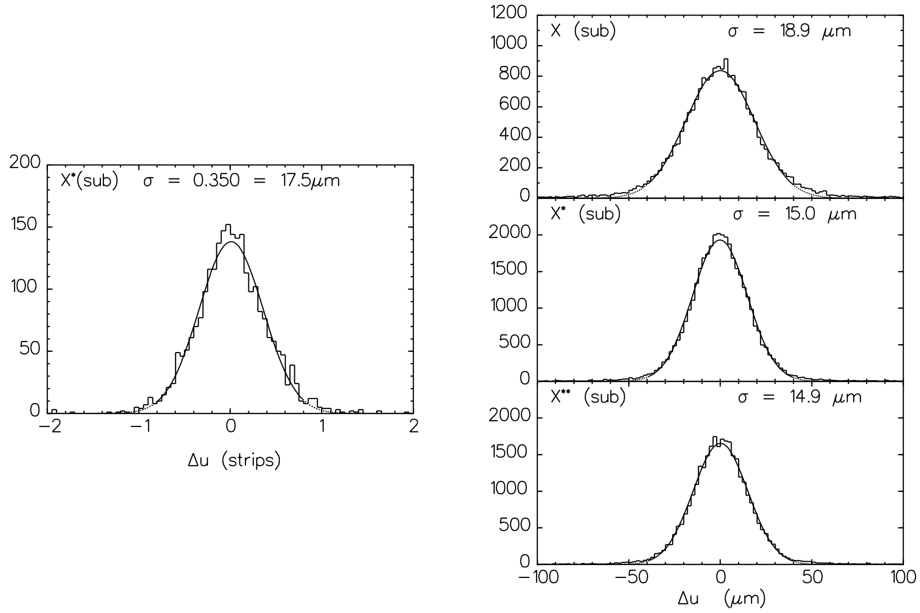

Figure 23: The resolution as predicted by the model (left) and according to the data (right) for strips on the substrate side of the X detector.

- the prediction, understanding, and explanation of the "bumps and wiggles" seen in the strip response function plot when strips are on the growth side; and
- a reasonably accurate prediction for the resolution of the detectors.

Additionally, the realizations that there is not a simple, linear relationship between mean path length and induced signal, and that the mean path length is a somewhat more fundamental quantity than the collection distance, are also important.

Some of the questions remain open:

- What actually happens when electrons hit in between strips?
- By how much does λ_q need to be increased in order to get significantly better resolution?
- For a given λ_q, is there a simple way to find the optimal thickness of the detector?
- Or, in reverse, if the thickness of the detectors must be fixed for other reasons, what is the optimal average mean path length, and can its spatial variation still be used as an advantage?

3.5 DB39

The DB39 detector is approximately 1100 μm thick and has a average mean path length of about 250 μm. Strip pitch is again 50 μm and strip width is 25 μm. Because a considerable amount of material has been lapped off of both the substrate and growth sides, the mean path length is not longer expected to be zero at one side of the detector.

Despite the apparent success of the model in making predictions for the X detector, it has been unable to make accurate predictions for DB39. It would therefore seem that either the model does not work properly, or that our understanding of a detector as thick as DB39 is incomplete. Due to considerable strip response irregularity and behaviors much different from expectations, the understanding of the detector is somewhat more suspect than is the model. Future studies with the model will hopefully answer whether or not polarization or crystal structure could explain some of the odd phenomena observed in this detector.

4 Acknowledgements

My eternal gratitude is owed to my advisor and mentor Professor John Conway for providing many of the ideas and strategies of the model, as well as for providing all of the experimentally derived plots. Professor Sunil Somalwar is responsible for the suggestion of using the weighting field method. Bob Stone and Professor Steve Schnetzer are responsible for keeping me and Professor Conway on the right track. I would also like to thank Professor Gordon Thomson for making us check our factors of two.

A Fourier expansion of the potential

In order for the relaxation method to be at all effective, a good first approximation for the electric field must be available. The method of separation of variables may be used to obtain this first approximation. Although the boundary conditions of interest are quite complicated and make an exact solution impossible, many approximations can be made to make the problem approximately solvable. First, instead of taking the true weighting field arrangement of one strip of width w at unit potential with many surrounding strips at ground, it may be assumed (since only an approximation is being made) that strip width equals strip pitch equals $2w$. This gives a boundary condition for the potential, $V = 1$ at $-w \leq x \leq w$ and $z = 0$, and $V = 0$ on all other boundaries (other strips, the solid electrode, and everywhere far away from the region of interest).

From standard arguments for separable solutions, one obtains as a general solution,

$$V(x, z) = \sum_{n=0}^{\infty} a_n \cos \frac{n\pi x}{L}(b_n e^{\frac{n\pi z}{L}} + c_n e^{\frac{n\pi z}{L}}) \tag{8}$$

where x is the dimension perpendicular to the length of the strips, z is into the depth of the detector, and L is a distance in x much greater than the region of interest. The reader can easily verify that Equation 8 satisfies Laplace's equation, $\nabla^2 V = 0$. No y dependence is assumed.

The boundary condition in z may be written as $V(z{=}t) = 0$, where t is the thickness of the diamond, for the solid electrode side, and as $V(z{=}0) = f(x)$ where

$$V(x, z{=}0) = f(x) = \begin{cases} 1 & |x| \leq w \\ 0 & \text{otherwise} \end{cases} \tag{9}$$

for the strip side, where w is the half width of a strip.

The first boundary condition tells us that $c_n = -b_n$, or

$$V(x, z) = \sum_{n=0}^{\infty} a_n \cos \frac{n\pi x}{L} \sinh \frac{n\pi(t - z)}{L} \tag{10}$$

where several factors independent of x and z have been absorbed into the constant a_n.

Using the second boundary condition a complete solution may be found by Fourier expansion of $f(x)$. The final result gives

$$V(x, z) = \frac{w}{L}(1 - \frac{z}{t}) + \sum_{n=1}^{\infty} \frac{2}{n\pi} \sin \frac{n\pi w}{L} \cos \frac{n\pi x}{L} \frac{\sinh \frac{n\pi(t-z)}{L}}{\sinh \frac{n\pi t}{L}} \tag{11}$$

where the factor $(1 - z/t)$ arises from using L'Hôpital's Rule for

$$\lim_{n \to 0} \left\{ \sinh \frac{n\pi(t - z)}{L} / \sinh \frac{n\pi t}{L} \right\} \quad . \tag{12}$$

References

[1] A. Peisert. *Silicon Microstrip Detectors*. 1992. In F. Sauli (ed.): *Instrumentation in high energy physics*. 1-79.

[2] S. Zhao. *Characterization of the Electrical Properties of Polycrystalline Diamond Films – A Dissertation*. Ohio State University. (1994)

[3] V. Radeka, Ann. Rev. Nucl. Part. Sci. **38** (1988) 217-77.

[4] D. N. de G. Allen. *Relaxation Methods*. McGraw-Hill, New York. (1954)

[5] S. K. Kim et al., Nuc. Instr. and Methods in Physics Research **A315** (1992) 39-42.

[6] W. Shockley. *Electrons and Holes in Semiconductors*. D. Van Nostrand Company, Inc., New York. (1950) 299-301, 349.

[7] L. S. Brown and D. L. Nordstrom, eds. Phys. Rev. D – Particles and Fields. *Review of Particle Properties*. sec. 12. (1994)

[8] M. Walsh. *Further studies of DBDS-39 in the November 1996 Beamtest*. Internal RD-42 note (1997)